

# Conformation and dynamics of 8-Arg-vasopressin in solution

Elke Haensele<sup>a</sup>, Lee Banting<sup>a</sup>, David C. Whitley<sup>a</sup>, and Timothy Clark<sup>\*,a,b</sup>

<sup>a</sup>E. Haensele, Dr. L. Banting, Dr. D. C. Whitley, Prof. Dr. T. Clark

Centre for Molecular Design, School of Pharmacy and Biomedical Sciences; University of Portsmouth, Portsmouth PO1 2DT (United Kingdom)

<sup>b</sup>Prof. Dr. T. Clark

Computer-Chemie-Centrum and Interdisciplinary Center for Molecular Materials; Friedrich-Alexander-Universität Erlangen-Nürnberg, Nögelsbachstraße 25, 91052 Erlangen (Germany);

Fax: (+49) 9131 8526565; E-mail: tim.clark@port.ac.uk

Supporting information for this article is available.

## Abstract

Arginine-vasopressin has been subjected to a long (11  $\mu$ s) molecular-dynamics simulation in aqueous solution. Analysis of the results by DASH and principal components analyses reveals four main ring conformations that move essentially independently of the faster-moving tail region. Two of these conformations (labeled “saddle”) feature well-defined  $\beta$ -turns in the ring and conserved transannular hydrogen bonds, whereas the other two (“open”) feature neither. The conformations have been identified and defined and are all of sufficient stability to be considered candidates for biologically active conformations in their cognate receptors.

## Keywords

vasopressin – molecular dynamics – DASH analysis – peptides – principal component analysis

## Introduction

8-Arginine-vasopressin (AVP, also known simply as vasopressin (VP), antidiuretic hormone (ADH) or argipressin), one of the first biologically active peptides to be synthesized by du Vigneaud in 1954<sup>1</sup>, is a nonapeptide with a six-membered cyclic moiety (Cys<sup>1</sup>-Tyr<sup>2</sup>-Phe<sup>3</sup>-Gln<sup>4</sup>-Asn<sup>5</sup>-Cys<sup>6</sup>) closed by a Cys<sup>1</sup>-Cys<sup>6</sup> disulfide bridge, and an  $\alpha$ -amidated three residue tail (Pro<sup>7</sup>-Arg<sup>8</sup>-Gly<sup>9</sup>-NH<sub>2</sub>).

AVP is a neurohypophyseal hormone and belongs to the vasopressin family of the evolutionary lineage vasotocin-vasopressin. Vasopressin-like hormones are found in all vertebrates, with AVP being the mammalian form. They all possess a basic amino acid, such as arginine or lysine, in position eight and are all involved in water homeostasis (for reviews see *inter alia*<sup>2</sup>).

AVP is synthesized in the magnocellular neurons of the posterior pituitary gland<sup>3</sup> complexed with neurophysin (NP), its carrier protein<sup>4</sup>. The function of NP is to target, package and store AVP before release into the bloodstream<sup>2b</sup>. The receptors activated by AVP belong to the transmembrane G-protein coupled receptor (GPCR) superfamily<sup>2a</sup>.

Once secreted into the blood stream, AVP is implicated in myriad physiological functions within the endocrine and neurocrine systems. Examples of its hormone function in addition to water homeostasis<sup>2</sup> include regulation of blood pressure<sup>5</sup>, antipyretic<sup>6</sup> and analgesic effects<sup>7</sup>. AVP acts as secretagogue for adrenocorticotropin<sup>2b,8</sup>, glucagon and insulin<sup>9</sup>. The peptide is thought to mediate social and sexual behavior, especially aggression, anxiety and pair-bonding<sup>10</sup>. Furthermore, AVP is believed to enhance memory and facilitate learning<sup>2b</sup> and to be involved in the pathophysiology of clinical disorders such as autism<sup>11</sup>, and may even play a role in circadian rhythm misalignments, like jet lag<sup>12</sup>.

Lowered AVP release in humans effects an increased blood sodium concentration (hypernatremia), excessive urine production (polyuria) and thirst. This may in turn lead to diabetes insipidus treatable by administration of AVP and AVP analogs<sup>13</sup>. In contrast, heightened AVP release causes hyponatremia, which may result in brain diseases and lung cancer<sup>14</sup> and can be treated with AVP-receptor antagonists<sup>15</sup>. AVP can be used in emergency medicine as an alternative to epinephrine in the event of cardiac arrest<sup>16</sup>.

To date, the only fully resolved crystal structure of AVP is as part of a trypsin complex (PDB ID: 1YF4)<sup>17</sup>. This structure contains a remarkably different backbone conformation to those found for the closely related peptide hormones 8-Lys-vasopressin (LVP, PDB ID: 1JK4<sup>4</sup>) and oxytocin (OT, PDB ID: 1NPO<sup>18</sup>) in their NP-complexes in the solid state.

The conformational characteristics of the peptide structures in the physiologically relevant neurophysin-complexes are a saddle-like ring with  $\beta$ -turns involving residues 3,4/4,5 and a high occurrence of transannular hydrogen bonds, primarily between Tyr<sup>2</sup>O and Asn<sup>5</sup>NH (*cf.* Scheme 1b). The tripeptide tail is only resolved in the OT-NP complex (PDB ID: 1NPO) where it is folded and possibly stabilized by a hydrogen bond Cys<sup>6</sup>O-Gly<sup>9</sup>NH (*cf.* Scheme 2b).

NMR studies suggest rapid interchange between the  $\beta$ -turn conformations of AVP in solution, although a folded (**saddle**) geometry appears to be maintained<sup>19</sup>. The polarity of the solvent seems only to affect formation of intramolecular hydrogen bonds. In DMSO, a hydrogen bond is indicated between Tyr<sup>2</sup>O and Asn<sup>5</sup>NH<sup>19</sup> but apparently not in water<sup>20</sup>. Studies in SDS micelles suggest the hydrophilic regions of the ring interact with a membrane, while the hydrophobic tail is exposed to the aqueous phase. Again, in this study the cyclic backbone of the AVP ring attached to the micelles appears similar to the NP-complexed form<sup>21</sup>.

These saddle-like conformations with a strongly puckered ring and the  $\beta$ -turns mentioned above have been confirmed computationally as “low-energy conformations” *inter alia* by Liwo *et al.*<sup>22</sup> via Monte Carlo and molecular-dynamics simulations.

In contrast, the conformation of AVP within the trypsin complex (PDB ID: 1YF4) is characterized by an unfolded, more planar ring conformation, here designated as “open”, with no significant internal hydrogen bonds and an extended tail (*cf.* Scheme 1a). AVP is an efficient inhibitor of trypsin<sup>17</sup>, although this is not known to be a true physiological function of AVP. The **open** conformation adopted in this trypsin complex can nevertheless be regarded as a bioactive conformation.

To our knowledge, little attention has been paid to an **open** conformation or its potential role in receptor binding with the vasopressin-receptor V2R<sup>23</sup>.

The V2R agonist-binding-pocket, common to all VP and OT receptor types, is located in a cleft within the transmembrane (TM) domains and AVP has been proposed to be almost completely buried within the receptor channel<sup>23,24</sup>. The hydrophobic ring-residues (Cys<sup>1</sup>-Tyr<sup>2</sup>-Phe<sup>3</sup>) are predicted to interact with residues of the TM-helices to activate signal

transduction, while the tail points outside the TM-core, interacting with an extracellular loop via its hydrophilic residue Arg<sup>8</sup>. The interaction between Arg<sup>8</sup> and the extracellular loops is also thought to be a key in receptor recognition<sup>2a,25</sup>.

Current models for interactions of peptide hormones with their receptors suggest multi-step mechanisms in which the peptide first contacts the cell membrane and then diffuses to the receptor until it finally finds its position to trigger receptor activities<sup>26</sup>. These events are probably accompanied by conformational changes of the ligand and concomitant allosteric effects on the receptors<sup>27</sup>. A flexible ligand exists in solution as an equilibrium involving several conformations of differing bioactivities. A conformation that has not yet been recognized with “slow” experimental techniques, such as NMR, might nevertheless be the important conformation for triggering biological effects such as receptor recognition and activation or inhibition<sup>27,28</sup>.

Thus, we have now investigated the conformational dynamics of this peptide in solution in depth with modern computational methods and analysis tools with special regard to the **open** conformation, which is evident in the largely ignored 1YF4 X-ray structure of AVP and is significantly different from the known **saddle** conformation.

Molecular-dynamics (MD) simulations have proven to be an accurate tool for describing the atomistic details of the conformational dynamics of biological systems in solution (*e.g.*<sup>29</sup>). Rapidly developing computational methods, increasing computational performance and improved force fields now make it possible to reveal new structural aspects of systems such as AVP, especially because microsecond simulations are now possible for a peptide of this size.

We now report an unrestrained 11  $\mu$ s MD simulation of the AVP-1YF4-peptide in explicit water solvent at 300 K using AMBER 10<sup>30</sup> and a detailed analysis of the resulting conformational space with several analysis tools contained in Ptraj<sup>31</sup> and DASH<sup>32</sup>, a fast conformational analysis tool for MD simulations developed especially for long trajectories for which classical clustering algorithms scale poorly.

## Methods

### Molecular dynamics simulation

The AMBER10 program suite<sup>30</sup> was used to optimize geometries and for the MD simulations. The X-ray structure of AVP from the trypsin complex (PDB ID: 1YF4)<sup>17</sup> was chosen as the initial conformation. The peptide was placed in a truncated octahedron water box (box size (XYZ) = 38.97 Å<sup>3</sup>) using the TIP4P-Ew water model<sup>33</sup>. Two chloride counterions were added to neutralize the system. The simulation system consisted of a total of 4,792 atoms, including 1,162 4-site water molecules and 142 AVP atoms.

The system was optimized using 500 steps of steepest-descent optimization followed by 8,945 of conjugated-gradient minimization at constant volume.

Molecular dynamics simulations were carried out using the AMBER ff99SB force field<sup>34</sup> under constant temperature (T = 300 K, Berendsen coupling<sup>35</sup> of 1.0 ps to an external heat bath) and constant pressure (p = 1 atm) periodic boundary conditions with a non-bonded cut off of 8 Å. The SHAKE<sup>36</sup> algorithm was employed for hydrogen atoms with a simulation time step of 2 fs. Energies were calculated using the Particle Mesh Ewald method<sup>37</sup> and coordinate 'snapshots' were written every picosecond. AVP was simulated in explicit water at 300 K for 11 μs.

### DASH analysis

Conformational clustering was performed with DASH, Version 2.10.<sup>32</sup> DASH is a fast conformational analysis tool for MD simulations developed especially for long trajectories for which classical pairwise distance-metric clustering algorithms (Cα) scale poorly. It analyses time-series of torsion angles, *e.g.* the trajectories of the Φ/Ψ dihedral angles of the protein/peptide backbone during the MD simulation. The result is a time series of DASH states called a DASH state trajectory. A DASH state is simply an ensemble of torsion angles that is representative for a main conformation (equivalent to a conformational cluster). No predetermined number of states is required, in contrast to clustering algorithms that use a similarity matrix, such as those implemented in AMBER tools<sup>31</sup>. A conformation must persist for a minimum number of time steps before it is identified as a DASH state, which gives an accurate representation of significant conformational changes. The DASH software is

released under the terms of the GNU General Public License and can be downloaded from the University of Portsmouth website<sup>38</sup>.

## Principal component analysis

The principal component (PC) analysis (PCA) was conducted using the dihedral angles extracted from the simulation (11,000 snapshots) using SAR-caddle<sup>39</sup>. Kaiser's eigenvalue-one test<sup>40</sup> was used to determine the number of significant PCs. Weights are simply the squares of the coefficients of the torsional angles in the relevant PC.

Further details of the calculations and analyses are given in the Supporting Information.

## Results and discussion

### Ring conformations

#### *Trajectory (transitions)*

An 11  $\mu$ s MD simulation of AVP in solution reveal the high conformational flexibility and fluctuation of this peptide (see Video S 1). Figure 1a shows the trajectory of conformational changes of the C $\alpha$ -backbone atoms 1 to 9 of AVP as root mean square deviation (RMSD) from the minimized starting conformation (PDB ID: 1YF4). Average RMSD values of distinct time-windows from the trajectory are given in Table 1. Significant RMSD changes indicate significant conformational changes, but despite a high fluctuation, there are only few substantial RMSD changes during the 11  $\mu$ s MD simulation. The most obvious transition is at 1.46  $\mu$ s. Limiting the RMSD calculation either to the ring (Fig. 1b) or to the tail C $\alpha$ -atoms (Fig. 1d) shows that the major overall transition of the peptide (Fig. 1a) corresponds to a change of the ring conformation. The radius of gyration of the ring system (Figure 1c) reveals further distinct transitions between differently folded ring conformations at 5.90, 6.43 and 7.19  $\mu$ s. The tail, however, fluctuates with a much higher frequency, apparently between two conformational states that are distributed evenly over the simulation. The video clip (Video S 1) suggests that these two tail states may be assigned to an extended state (Scheme 2a), in which the tail points away from the ring, and a folded state (Scheme 2b) in which the tail turns towards the lower face of the ring. The high frequency of transitions

between the two tail states indicates a high flexibility of the tail, significantly higher than the ring.

#### *DASH state analysis*

A DASH analysis of all 16  $\Phi/\Psi$  dihedral angles (T16) of the AVP backbone ( $C\alpha$  2 to 9) during the 11  $\mu\text{s}$  MD simulation results in 35 conformational states. Every DASH state represents, like a cluster, a conformation that is representative for an ensemble of similar backbone conformations. The 35 overall states can be clustered into four groups of states with common structural characteristics for the cyclic part of the peptide (Fig. 2a-d) and a fifth group of states (“variants”, Fig. S1 and Table S1) that does not match one of the main groups. This fifth group occurs between 5.90 and 6.43  $\mu\text{s}$ . A detailed table of the sequence of DASH states (DASH state trajectory) during the 11  $\mu\text{s}$  simulation is available as Supplementary Material (Table S2).

#### *DASH ring-state analysis*

As the RMSD trajectories suggest that the tail movements do not affect the main ring conformation, we first focused the DASH analysis on the ring dihedrals  $\Phi/\Psi$  2 to 6 (T10). Each DASH state now represents an ensemble of similar ring-backbone conformations shown in Figure 3 and Table 2. In order to distinguish between DASH overall states and DASH ring states, DASH overall states are denoted as T16 and DASH ring states as T10.

The initial 35 overall states are now reduced to twelve ring states. These ring states can be assigned clearly to the main time-windows of the trajectory between the transitions at 1.46, 5.90, 6.43, and 7.10  $\mu\text{s}$  (Fig. 1a-c). Furthermore, analyzing the T10 and T16 DASH state trajectories (Fig. 4, Table S2), shows that each overall state can be assigned to a distinct ring state (see Table 2). In other words, each overall state can be considered as a main ring conformation combined with a distinct tail-conformation, as will be discussed in detail below. Table 2 shows absolute and relative populations of overall and ring states and how they correspond. Absolute populations refer to the total simulation time of 11  $\mu\text{s}$  and relative populations refer to the individual lengths of a conformational time-window. The main ring conformations and the corresponding main windows are denoted as (a) **open** (0 to 1.46  $\mu\text{s}$ ), (b) **saddle** (1.46 to 5.90  $\mu\text{s}$ ), (c) **clinched open** (6.43 – 7.19  $\mu\text{s}$ ) and (d) **twisted saddle** (7.19 to 11 $\mu\text{s}$ ) to reflect common structural characteristics. The fifth window

identified on the RMSD plot between 5.90 and 6.43  $\mu$ s contains variants of the main ring conformations and will not be discussed in detail here. This work is focused on AVP's main conformational states, which correspond to the four main trajectory windows. Other, short-lived states are observed during the simulation, but do not play a significant role and will only be defined in the Supporting Information.

#### *Populations of the conformations*

The four main ring conformations (***open***, ***saddle***, ***clinched open*** and ***twisted saddle***) are present for more than 95% of the simulation time. As a result of the DASH ring analysis, every conformational group is represented by two ring states (T10), a main state with a relative population of up to 94% and a less populated state. Both major and minor states are present for 95 to 100% of the relevant time-window. Figure 3 shows the C $\alpha$  1 to 6 alignment of the ring states for each main ring conformation. Frequent interconversions between the representative states occur within each main conformational window. The DASH state mean angles (Table 3, Fig. S 2) reveal that the major and minor ring-states of a distinct conformational group (***open*** or ***saddle***) differ significantly (more than 60°) for only one torsional angle. This is  $\Phi_6$  for the ***open*** and ***saddle*** (differences of 72° and 66°, respectively; only 52° for ***twisted saddle*** and 35° for ***clinched open***) states and  $\Psi_5$  (73°) for the ***clinched open*** states. The DASH state mean angles (Table 3, Fig. S2) reveal that the major and minor ring-states of a distinct conformational group (***open*** or ***saddle***) differ in only one torsion. This is  $\Phi_6$  for the ***open***, ***saddle*** and ***twisted saddle*** states and  $\Psi_5$  for the ***clinched open*** states. These result in different disulfide-bridge conformations for each state. Although the disulfide-bridge torsions were not included in the DASH ring-state analysis, their conformations are probably characteristic (see Fig. 3a-d, disulfide-bridges are shown as lines). RMSD differences between states of the same ring conformation are small,  $\leq 0.25$  Å, in comparison to RMSD differences between states of different ring conformations, 0.9 to 2.2 Å (Table S3). The ***saddle*** and the ***twisted saddle*** ring conformations are the most populated structures, with absolute populations of 40 and 35%, respectively. The open conformations, ***open*** and ***clinched open***, occur only 13 and 7% of the time.

#### *Secondary structure and hydrogen bonds*

The secondary structure was determined by means of ring-internal turn propensities, turn types and hydrogen bonds. Turn propensities and hydrogen-bond occupancies were



calculated using AMBER tools, and turn types were identified by comparing the DASH mean-angles with ideal  $\beta$ -turn type torsions. Turn propensities and hydrogen-bond populations are given in Table 4 and Table 5 and the torsion-angle ensembles for every main DASH ring state in Table 3 and the results are illustrated in Scheme 1.

The **saddle** (Scheme 1b, Fig. 3b) and related **twisted saddle** (Scheme 1d, Fig. 3d) ring conformations are the most highly populated, occurring for 75% of 11  $\mu$ s (Table 2). Both feature a highly populated (more than 90%) turn at residues Phe<sup>3</sup> and Gln<sup>4</sup>. The **saddle** is characterized by a further turn centered at Asn<sup>5</sup> (89%). This turn also occurs in the **twisted saddle** but is less highly populated (62%). The DASH-state mean-angles (Table 3 and S 4) reveal a  $\beta$ -turn type I centered at 3,4 for the **saddle** conformation in addition to a slightly distorted  $\beta$ -turn type I centered at 4,5. These  $\beta$ -turns are stabilized by highly populated (83-96%) hydrogen bonds between the carbonyl-oxygen of Tyr<sup>2</sup> (Tyr<sup>2</sup>O) and the amide-hydrogen of Asn<sup>5</sup> (Asn<sup>5</sup>NH), and between Tyr<sup>2</sup>O and Cys<sup>6</sup>NH. In the **twisted saddle** ring-conformation, however, only the Tyr<sup>2</sup>O-Asn<sup>5</sup>NH hydrogen bond is highly populated (83%) and the 3,4 centered turn is now a classical  $\beta$ -turn type II. The difference between a  $\beta$ -turn type I and type II is simply the orientation of the central peptide bond 3,4. The **twisted saddle** conformation shows a slight tendency to form a Tyr<sup>2</sup>NH-Asn<sup>5</sup>O hydrogen bond (7% occupancy). A Tyr<sup>2</sup>NH-Asn<sup>5</sup>O hydrogen bond has also been suggested on the basis of NMR experiments<sup>19</sup>. A rearrangement from **saddle** to **twisted saddle** or changing the 3,4  $\beta$ -turn from type I to type II twists the ring making it more open (*cf.* radius of gyration, Fig. 1c), whereas the main orientation of the side chains 2 to 4 remains unchanged. This may be necessary to facilitate AVP entry and/or fit into different GPCR pockets.

There is no direct transition between **saddle** and **twisted saddle** in the 11  $\mu$ s MD, suggesting that interconversion of the two ring conformations may occur via one or more conformational intermediates, *e.g.* the **clinched open** conformation or the variants that are observed between 5.90 and 6.43  $\mu$ s.

The relatively sparsely populated **clinched open** ring conformation (Scheme 1c, Fig. 3c) is significantly less folded than the two **saddle** conformations but more than the **open**. The most highly populated intramolecular hydrogen-bond is Phe<sup>3</sup>O-Cys<sup>6</sup>NH (28%, Table 5) and turns centered at Gln<sup>4</sup> and Asn<sup>5</sup> occur about half of the time (46%, Table 4). Loosely defined turns are thus more likely than ideal  $\beta$ -turns. The DASH ring-state mean-angles show a very high fluctuation of  $\Psi$  5 (standard deviation =  $\pm 61^\circ$ , Table 3) so unambiguous turn-type

assignment is not possible. The **clinched open** ring structure can be classified as a flexible ring conformation with a tendency to form a  $\beta$ -turn type VIII or type I centered at 4,5.

Finally, the **open** ring conformation, the starting conformation for the simulation, shows none of the ideal turn structures (Scheme 1a, Fig. 3a). There is a slight tendency to center ring turns at residues Tyr<sup>2</sup> and Phe<sup>3</sup> (20%, Table 5) accompanied by sparsely populated hydrogen bonding-interactions of Tyr<sup>2</sup>O and Gln<sup>4</sup>NH (39%), and Cys<sup>1</sup>O and Gln<sup>4</sup>NH (12%). Summarizing, this ring conformation can be readily classified as **open** as it has no significantly populated intramolecular hydrogen bonds and no defined  $\beta$ -turns.

#### *Transition key torsions*

A torsion angle is defined as a key torsion if its value changes significantly ( $> 90^\circ$ ) from one ring conformation to another. Fig. 5 shows the differences of the mean torsions for the main ring conformations **open**, **saddle**, **clinched open** and **twisted saddle** represented by the main ring states (T10, Table 2). Only dihedrals  $\Phi$  2,  $\Phi$  5 and  $\Phi/\Psi$  6 do not show large differences, all other torsions can be qualified as key torsions for interconversions between the main ring conformations. A complete list of key torsion angle differences between main ring conformations is given in Table S5. Direct transitions only occurred between (i) **open** and **saddle** and (ii) **clinched open** and **twisted saddle**. The key torsions for these transitions are (i)  $\Phi$  3,  $\Psi$  4,  $\Psi$  5 (Scheme 3a,b) and (ii)  $\Psi$  2,  $\Phi$  4,  $\Psi$  5 (Scheme 3c,d). Changes of these torsions correlate with rotations of the corresponding peptide bonds and the relative orientation of carbonyl oxygens and amide hydrogens, and elucidate the mechanism of interconversions.

For example, to convert **open** to **saddle**, the Tyr<sup>2</sup> carbonyl-oxygen and the amide hydrogens of Asn<sup>5</sup> and Cys<sup>6</sup> should point into the ring. Torsions  $\Phi$  3,  $\Psi$  4 and  $\Psi$  5 are the key torsions responsible for turning these atoms into the ring and thus to enable the characteristic intramolecular hydrogen bond to be formed. To interconvert from **clinched open** to **twisted saddle**, the hydrogen bond Phe<sup>3</sup>O-Cys<sup>6</sup>NH must be replaced by one between Tyr<sup>2</sup>O and Asn<sup>5</sup>NH. This is accomplished by rotating  $\Psi$  2 and  $\Phi$  4, which turns Tyr<sup>2</sup>O into the ring displacing Phe<sup>3</sup>O. A concomitant rotation of  $\Psi$  5 causes Cys<sup>6</sup>NH to turn thereby weakening the hydrogen bond between Phe<sup>3</sup>O and Cys<sup>6</sup>NH. These ring interconversions have so far proved too complex for their thermodynamics to be determined by simple umbrella sampling and are therefore now being investigated using dual-topology thermodynamic integration.

### Disulfide bridge

One remaining important feature of the ring conformations is the chiral disulfide dihedral  $\chi_3$  ( $\angle \text{Cys}^2\text{C}\beta\text{-Cys}^2\text{S-Cys}^6\text{S-Cys}^6\text{C}\beta$ ), Figure 6 shows the dynamics of this torsion. The disulfide bridge adopts two main conformations for  $\chi_3$  with average values of either  $+88.9^\circ$  (g) or  $-86.6^\circ$  (g'). Interconversions between these two states do not necessarily correspond to transitions between different time-windows of the ring conformations but are rather frequent independent occurrences. Each main ring conformation can exhibit conformations of the disulfide bridge conformations with negative and positive dihedrals. Transitions between these disulfide conformations occur independently of the main ring conformation. The positive torsion angle is favored by 78.2 to 21.8% and is consistent with experimental evidence (see *e.g.*<sup>41</sup>). The simulation suggests that g/g' transitions are more frequent for *open* ring conformations than for *saddle*.

### Tail conformations

As described above, the RMSD trajectory of the C $\alpha$  7 to 9 segment (Fig. 1d) suggests two equally distributed main conformations for the tail, whereas the DASH analysis of the *tail* dihedrals  $\Phi/\Psi$  7 to 9 allows these dynamic conformations to be classified in detail. The results are given in Table 6, Scheme 2 and Figure 7. There are six distinct tail states (**T6**) that reveal two major tail conformations, (i) an *extended* tail conformation with no significant turns, and (ii) a tail conformation with a 7,8  $\beta$ -turn type II, here denoted as *folded*. Each main conformation is represented by two DASH states, differing in torsions  $\Phi/\Psi$  9 (Fig. S3). These torsions are only responsible for the orientation of the C-terminal CONH<sub>2</sub>-group and do not affect the *extended* or *folded* conformation.

AVP favors the *extended* conformation of the tail significantly with an absolute population of 81% during the simulation vs. 17% for the *folded* 7,8  $\beta$ -turn type II conformation. The preference for the *extended* tail conformation is most likely due to the bulky residue Arg<sup>8</sup>, which causes steric clashes when the tail is *folded*.

Two further transient conformations can be identified, a hybrid tail conformation (absolute population 2.0%), which is not completely extended but has no defined folding, and a 7,8  $\beta$ -turn type I structure (absolute population 0.8%).

Figure 4 shows the DASH state trajectories for all *overall* states (**T16**), *ring* states (**T10**) and *tail* states (**T6**). There are 176 transitions between the six **T6** tail-states but only 77

transitions between the twelve **T10** *ring*-states, confirming that the tail is significantly more flexible than the ring. The most striking result, however, is that the *tail* states do not correlate directly with *ring* states in terms of transitions or formation of distinct conformational groups. In fact, similarly to the two states of the disulfide bridge, all *tail* states are distributed evenly over the entire simulation independently of the ring conformation. This is shown convincingly by a principal component analysis of the torsion angles throughout the simulation. As is shown in Figure 8a, there are six significant principal components (PCs) according to the eigenvalue-one test, of which PCs 5 and 6 have eigenvalues just barely larger than unity and are therefore at best marginally non-trivial. Figure 8b shows the weights (squared coefficients) of the contributions of the individual torsions to PCs 1 and 2 and Figure 8c those of PCs 3 and 4. The former are clearly localized on the ring and the latter on the tail. The contributions of ring torsions in PCs 3 and 4 and of tail fluctuations in 1 and 2 are very small. Interactive 3D-plots of the first four PCs are given as HTML-pages in the Supporting Material. Interestingly, these show that the two twisted saddle states, although very similar, are clearly separated in PC-space. This separation is mostly due to PC2.

Thus, every *overall* state can be described in a modular manner as a combination of a *ring* and a *tail* state. The matrix of all main-state combinations found in this simulation is given in Table 7. Although the conformational changes of the ring and tail are not correlated, the relative populations of **extended** and **folded** tail-states vary depending on the *ring* conformation (see Table 6). The highest preference for a **folded** tail is found for the **clinched open** ring (26% relative population), the lowest (5%) for an **open** ring conformation. The **saddle** and **twisted saddle ring** conformations are found together with a **folded** tail 20 and 15% of their occurrence, respectively. Again, the sterically demanding Arg<sup>8</sup> residue is most likely responsible for these preferences; the propensity to form a folded tail depends on the available space.

## Conclusions

A single long (11  $\mu$ s) simulation of AVP in water has revealed details of its conformational behavior and possible biologically active conformations. Conformational changes on the MD

time scale are frustratingly slow, so that, even from the long simulation, we cannot estimate the free-energy difference between the ring conformations from their concentrations. However, the conformational rearrangements are clearly fast on the NMR time scale, in agreement with the experimental results.

The simulation reveals four distinct ring conformations that are essentially independent of the faster tail motions. The *saddle* and *twisted saddle* ring conformations exhibit  $\beta$ -turns centered at residues 3,4/4,5 as expected from experiments and are fixed by transannular hydrogen bonds. The alternative *open* and *clinched open* conformations do not feature transannular H-bridges. The *saddle* structure identified in the simulation corresponds closely to that found in crystal structure 1JK4.

The simulation is quite consistent with Sikorska and Rodziewicz-Motowidlo's NMR results<sup>20</sup>. They suggest two main conformations, both with 3,4  $\beta$  II-turns. One is proposed to exhibit a 4,5  $\beta$  III'-turn and the other a type I'-turn at this position. Our simulations also reveal turns at 3,4 and 4,5 to be dominant in aqueous solution. The 3,4  $\beta$ -turn type II is found in our *twisted saddle* conformation, but only with a sparsely populated 4,5 turn; a significantly high turn propensity at residues 4 and 5 is found in our *saddle* conformation but here in combination with a  $\beta$ -turn type I at residues 3 and 4. The two studies agree well about the tail conformation, which we found to be approximately 80% *extended*.

The *open* structure featured in the simulation corresponds closely to the AVP conformation found in the crystal structure of the trypsin complex (PDB ID: 1YF4) and features neither a well characterized  $\beta$ -turn nor conserved transannular hydrogen bonds. The *clinched open* conformation identified in the simulation is apparently new and probably represents an intermediate minority conformation involved in inter-*saddle* rearrangements.

In general, the simulation is compatible with the known experimental data, which allows us to be confident about its accuracy, even though it is limited to 11  $\mu$ s and exhibits only a few transitions between major rings states. Above all, the main conformations found can all be considered as candidates for biologically active conformations in different receptors as they are clearly easily accessible thermodynamically. We are now carrying out extensive thermodynamic integration studies to define the thermodynamics of the major conformations in solution.

Technically, DASH has proven to be an extremely useful and effective analysis tool for such simulations. In particular its beneficial scaling helps to analyze such long simulations. The

finding that the movements of the ring and the tail are largely independent facilitates the analysis considerably.

The conformational distribution demonstrated in this work can now serve as a basis for comparison with those simulated for AVP docked into receptor pockets and for extended simulations of NMR and circular dichroism spectra. Above all, however, MD simulations have proven once more to be useful, and perhaps the most powerful, tools for analyzing the conformational behavior of peptide hormones of comparable size to AVP.

## Acknowledgments

This work was supported by the European project “Peptide Research Network of Excellence” PeReNE as part of the Interreg IVA France (Channel) – England 2007-2014 program (Interreg EU). We thank Jonathan Essex (University of Southampton, UK) and Ronan Bureau (University of Caen, France) for helpful discussions and Harald Lanig (University of Erlangen, Germany) for support with the simulations. Work in Erlangen was supported by the Deutsche Forschungsgemeinschaft as part of Graduiertenkolleg 1910 “*Medicinal Chemistry of Selective GPCR Ligands*”.

## Glossary

abs	Absolute	PCA	Principle Component Analysis
AMBER	Assisted Model Building with Energy Refinement	PDB	Protein Data Bank
av	Average	RadGyr	Radius of Gyration
AVP	8-Arginine-Vasopressin	rel	Relative
cl.open	Clinched Open	RMSD	Root Mean Square Deviation
DASH	Dynamics Analysis by Salt and Hudson	SDS	Sodium Dodecyl Sulfate
DMS	Dimethyl Sulfate	StdDev	Standard Deviation
ff99sb	Force Field 1999 Stony Brooks	T10	DASH analysis of torsions $\Phi/\Psi$ 2 to 6 (10 torsions)
g/g'	gauche/gauche'	T16	DASH analysis of torsions $\Phi/\Psi$ 2 to 9 (16 torsions)
GNU	General Public License	TIP4P-Ew	Transferable Intermolecular Potential 4 Point -
GPCR	G-Protein Coupled Receptor	Ewald	
Hbond	Hydrogen Bond	TM	Trans Membrane
MD	Molecular Dynamics	tw.saddle	Twisted Saddle
NH	Amide Hydrogen	V2R	Vasopressin-2 receptor
NP	Neurophysin	O	Carbonyl Oxygen
OT	Oxytocin		
PC	Principle Component		

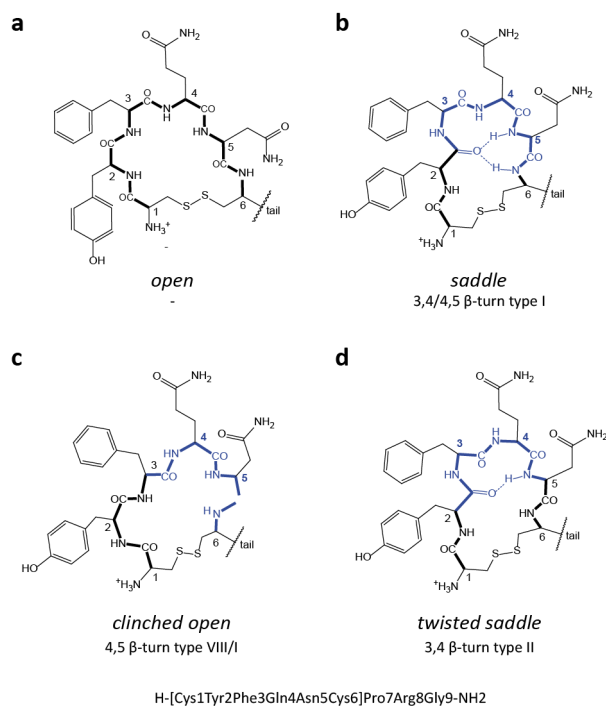
## References

- [1] du Vigneaud V, Gish DT, Katsoyannis PG (1954) A Synthetic Preparation Possessing Biological Properties Associated with Arginine Vasopressin. *J Am Chem Soc* 76:4751-4752
- [2] a) Laycock JF (2010) Perspectives on vasopressin. Imperial College Press, London, UK; b) Gimpl G, Fahrenholz F (2001) The oxytocin receptor system: structure, function, and regulation. *Physiol Rev* 81:629-683; c) Strand FL (1999) *Neuropeptides: regulators of physiological processes*. MIT Press, Cambridge, Mass, pp 229-265
- [3] Barberis C, Morin D, Durroux T, Mouillac B, Guillon G, Seyer R, Hibert M, Tribollet E, Manning M (1999) Molecular pharmacology of AVP and OT receptors and therapeutic potential. *Drug News Perspect* 12:279-292
- [4] Wu CK, Hu B, Rose JP, Liu ZJ, Nguyen TL, Zheng C, Breslow E, Wang BC (2001) Structures of an unliganded neurophysin and its vasopressin complex: implications for binding and allosteric mechanisms. *Protein science: a publication of the Protein Society* 10:1869-1880
- [5] a) Fujiwara Y, Tanoue A, Tsujimoto G, Koshimizu TA (2012) The roles of V1a vasopressin receptors in blood pressure homeostasis: a review of studies on V1a receptor knockout mice. *Clin Exp Nephrol* 16:30-34; b) Pittman QJ, Bagdan B (1992) Vasopressin involvement in central control of blood pressure. *Progress in brain research* 91:69-74
- [6] Pittman QJ, Wilkinson MF (1992) Central arginine vasopressin and endogenous antipyrasis. *Can J Physiol Pharmacol* 70:786-790
- [7] Mogil JS, Sorge RE, LaCroix-Fralish ML et al (2011) Pain sensitivity and vasopressin analgesia are mediated by a gene-sex-environment interaction. *Nat Neurosci* 14:1569-1573
- [8] a) Manning M, Misicka A, Olma A et al (2012) Oxytocin and vasopressin agonists and antagonists as research tools and potential therapeutics. *J Neuroendocrin* 24:609-628; b) Jard S (1998) Vasopressin receptors. A historical survey. *Adv Exp Med Biol* 449:1-13
- [9] Dunning BE, Moltz JH, Fawcett CP (1984) Modulation of insulin and glucagon secretion from the perfused rat pancreas by the neurohypophysial hormones and by desamino-D-arginine vasopressin (DDAVP). *Peptides* 5:871-875
- [10] Young LJ, Flanagan-Cato LM (2012) Editorial comment: oxytocin, vasopressin and social behavior. *Horm Behav* 61:227-229
- [11] Insel TR, O'Brien DJ, Leckman JF (1999) Oxytocin, vasopressin, and autism: is there a connection? *Biol Psychiatry* 45:145-157
- [12] Yamaguchi Y, Suzuki T, Mizoro Y, Kori H, Okada K et al (2013) Mice Genetically Deficient in Vasopressin V1a and V1b Receptors Are Resistant to Jet Lag. *Science* 342:85-90
- [13] Manning M, Chan WY, Sawyer WH (1993) Design of cyclic and linear peptide antagonists of vasopressin and oxytocin: current status and future directions. *Regulatory peptides* 45:279-283
- [14] a) Verbalis JG (2003) Disorders of body water homeostasis. *Best practice & research. Clin Endocrinol Metabolism* 17:471-503; b) Leichner RW, Greenberg A (2012) Hyponatremia and the use of vasopressin receptor antagonists in critically ill patients. *J Intensive Care Med* 27:207-218
- [15] Verbalis JG (2006) AVP receptor antagonists as aquaretics: review and assessment of clinical data. *Cleveland Clinic J Med* 73 Suppl 3:S24-33
- [16] Barlow M (2002) Vasopressin. *Emerg Med (Freemantle)* 14:304-314
- [17] Syed Ibrahim B, Patabhi V (2005) Trypsin inhibition by a peptide hormone: crystal structure of trypsin-vasopressin complex. *J Mol Biol* 348:1191-1198
- [18] Rose JP, Wu CK, Hsiao CD, Breslow E, Wang BC (1996) Crystal structure of the neurophysin-oxytocin complex. *Nat Struct Biol* 3:163-169
- [19] Schmidt JM, Ohlenschlager O, Ruterjans H et al (1991) Conformation of [8-arginine]vasopressin and V1 antagonists in dimethyl sulfoxide solution derived from two-dimensional NMR spectroscopy and molecular dynamics simulation. *Eur J Biochem* 201:355-371
- [20] Sikorska E, Rodziewicz-Motowidlo S (2008) Conformational studies of vasopressin and mesotocin using NMR spectroscopy and molecular modelling methods. Part I: Studies in water. *J Pept Sci* 14:76-84
- [21] Rodziewicz-Motowidlo S, Sikorska E, Oleszczuk M, Czaplowski C (2008) Conformational studies of vasopressin and mesotocin using NMR spectroscopy and molecular modelling methods. Part II: Studies in the SDS micelle. *J Pept Sci* 14:85-96
- [22] Liwo A, Tempczyk A, Oldziej S et al (1996) Exploration of the conformational space of oxytocin and arginine-vasopressin using the electrostatically driven Monte Carlo and molecular dynamics methods. *Biopolymers* 38:157-175

- [23] Czaplowski C, Kazmierkiewicz R, Ciarkowski J (1998) Molecular modeling of the human vasopressin V2 receptor/agonist complex. *J Comput Aided Mol Des* 12:275-287
- [24] Mouillac B, Chini B, Balestre MN et al (1995) The binding site of neuropeptide vasopressin V1a receptor. Evidence for a major localization within transmembrane regions. *J Biol Chem* 270:25771-25777
- [25] Barberis C, Mouillac B, Durroux T (1998) Structural bases of vasopressin/oxytocin receptor function. *J Endocrinol* 156(2):223-229
- [26] a) Schwyzer R (1995) In search of the 'bio-active conformation'--is it induced by the target cell membrane? *J Mol Recognit* 8:3-8; b) Mierke DF, Giragossian C (2001) Peptide hormone binding to G-protein-coupled receptors: structural characterization via NMR techniques. *Med Res Rev* 21:450-471
- [27] Changeux JP, Edelstein SJ (2005) Allosteric mechanisms of signal transduction. *Science* 308:1424-1428
- [28] a) Cui Q, Karplus M (2008) Allostery and cooperativity revisited. *Protein science: a publication of the Protein Society* 17:1295-1307; b) Gunasekaran K, Ma B, Nussinov R (2004) Is allostery an intrinsic property of all dynamic proteins? *Proteins* 57:433-443
- [29] Shao J, Tanner SW, Thompson N, Cheatham TE (2007) Clustering Molecular Dynamics Trajectories: 1. Characterizing the Performance of Different Clustering Algorithms. *J Chem Theor Comput* 3:2312-2334
- [30] Case DA, Darden TA, Cheatham II TE et al (2008) AMBER 10
- [31] Case DA, Darden TA, Cheatham II TE et al (2008) AmberTools 1.0
- [32] Salt DW, Hudson BD, Banting L et al (2005) DASH: a novel analysis method for molecular dynamics simulation data. Analysis of ligands of PPAR-gamma. *J Med Chem* 48:3214-3220
- [33] a) Jorgensen WL, Chandrasekhar J, Madura JD et al (1983) Comparison of Simple Potential Functions for Simulating Liquid Water. *J Chem Phys* 79:926-935; b) Horn HW, Swope WC, Pitnera JW et al (2004) Development of an improved four-site water model for biomolecular simulations: TIP4P-Ew. *J Chem Phys* 120:9665-9678
- [34] Hornak V, Abel R, Okur A et al (2006) Comparison of multiple amber force fields and development of improved protein backbone parameters. *Proteins Struct Funct Bioinf* 65:712-725
- [35] Berendsen HJC, Postma JPM, van Gunsteren WF et al (1984) Comparison of multiple amber force fields and development of improved protein backbone parameters. *J Chem Phys* 81:3684-3690
- [36] Ryckaert JP, Ciccotti G, Berendsen HJC (1977) Numerical-Integration of Cartesian Equations of Motion of a System with Constraints - Molecular-Dynamics of N-Alkanes. *J Comput Phys* 23:327-341
- [37] Darden T, York D, Pedersen L (1993) Particle Mesh Ewald - an N.Log(N) Method for Ewald Sums in Large Systems. *J Chem Phys* 98:10089-10092
- [38] DASH 1.0 (2008); Available from: [www.port.ac.uk/research/cmd/software](http://www.port.ac.uk/research/cmd/software).
- [39] SAR-Caddle, (2013) Cepos InSilico Ltd, Kempston, UK; Available from: [www.ceposinsilico.de/products/sar-caddle.htm](http://www.ceposinsilico.de/products/sar-caddle.htm)
- [40] Kaiser HF (1960) The Application of Electronic Computers to Factor Analysis. *Educ Psychol Meas* 20:141-151
- [41] Pazderková M, Bednářová L, Dlouhá H et al (2012) Electronic and vibrational optical activity of several peptides related to neurohypophyseal hormones: Disulfide group conformation. *Biopolymers* 97:923-932
- [42] a) Venkatachalam CM (1968) Stereochemical criteria for polypeptides and proteins. V. Conformation of a system of three linked peptide units. *Biopolymers* 6:1425-1436; b) Richardson JS (1981) The anatomy and taxonomy of protein structure. *Adv Protein Chem* 34:167-339
- [43] Kabsch W, Sander C (1983) Dictionary of protein secondary structure: pattern recognition of hydrogen-bonded and geometrical features. *Biopolymers* 22 (12):2577-2637



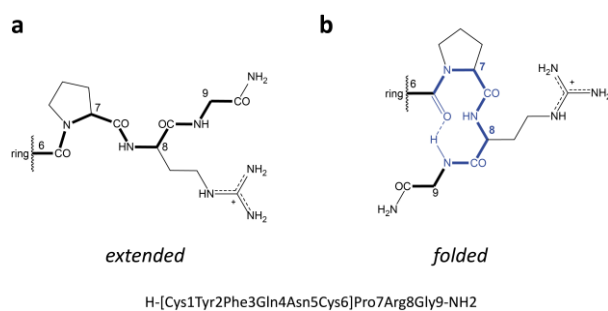
## Figure and schemes



### Scheme 1

Main conformational types of the cyclic part of 8-Arg-vasopressin (AVP)

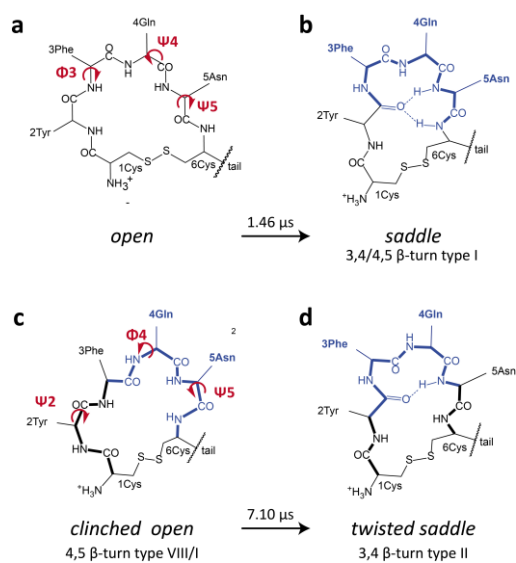
**(a) open:** no intramolecular hydrogen bonds and no classical  $\beta$ -turn types; **(b) saddle:**  $\beta$ -turn type I centered at 3,4,4,5 and stabilized by a transannular hydrogen bond from Tyr<sup>2</sup>O to Asn<sup>5</sup>NH and Cys<sup>6</sup>NH; **(c) clinched open:** minor propensity for  $\beta$ -turns type VIII or I centered at 4,5; **(d) twisted saddle:**  $\beta$ -turn type II centered at 3,4 with hydrogen bond Tyr<sup>2</sup>O to Asn<sup>5</sup>NH



## Scheme 2

Main conformational types of the N-terminal tail of AVP

**(a)** *extended* tail: no turns, no significantly populated hydrogen bonds; **(b)** *folded* tail:  $\beta$ -turn type II centered at residues 7 and 8, hydrogen bond from Cys<sup>6</sup>O to Gly<sup>9</sup>NH



**Scheme 3**

Key torsions for the interconversion of the main ring conformations of 8-Arg-vasopressin

**(a,b)** interconversion *open* to *saddle* at 1.46  $\mu\text{s}$  (11  $\mu\text{s}$  MD); **(c,d)** interconversion *clinched open* to *twisted saddle* at 7.10  $\mu\text{s}$  (11  $\mu\text{s}$  MD)

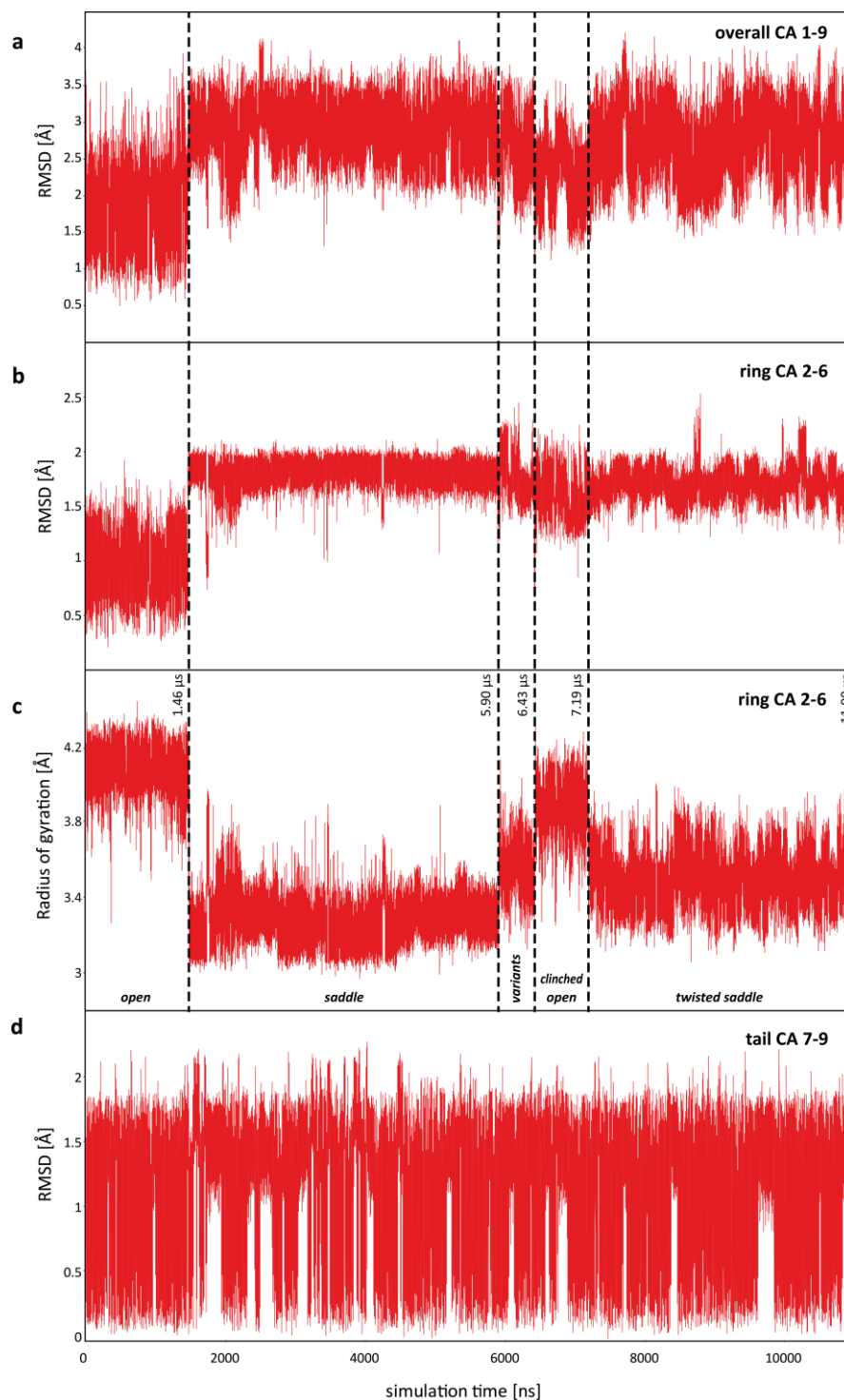


**Figure 1**

Root mean square deviations (RMSD) and radius of gyration (RadGyr) of 8-Arg-vasopressin during 11  $\mu$ s MD simulation (reference: minimized initial MD structure, AVP<sub>1VF4</sub>). **(a)** RMSD of C $\alpha$ -backbone atoms 1 to 9 (*overall*); **(b)** RMSD of C $\alpha$ -backbone atoms 2 to 6 (*ring*); **(c)** Radius of gyration of C $\alpha$ -backbone atoms 2 to 6 (*ring*); **(d)** RMSD of C $\alpha$ -backbone atoms 7 to 9 (*tail*). Dotted lines indicate significant changes of the RMSD/RadGyr and mark time-windows of different ring conformations (denoted as *open*, *saddle*, *variants*, *clinched open* and *twisted saddle*)

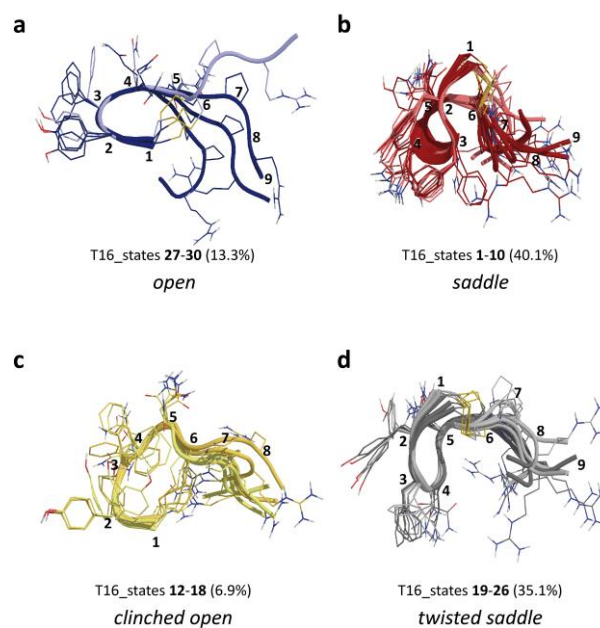


**Fig. 2**

Main overall conformations of 8-Arg-vasopressin

Representative states in water resulting from a DASH state analysis of backbone dihedrals  $\Phi/\Psi$  2 to 9. Absolute populations for every group of conformations are given in parenthesis and refer to 11  $\mu$ s MD

**(a)** Representatives with *open* ring conformation; **(b)** representatives with *saddle* ring conformation; **(c)** representatives with *clinched open* ring conformation; **(d)** representatives with *twisted saddle* ring conformation. Depiction: backbone = cartoon, side chains = lines, representatives are only labeled for the main populated state of each group. Residues are only labeled for each major populated state

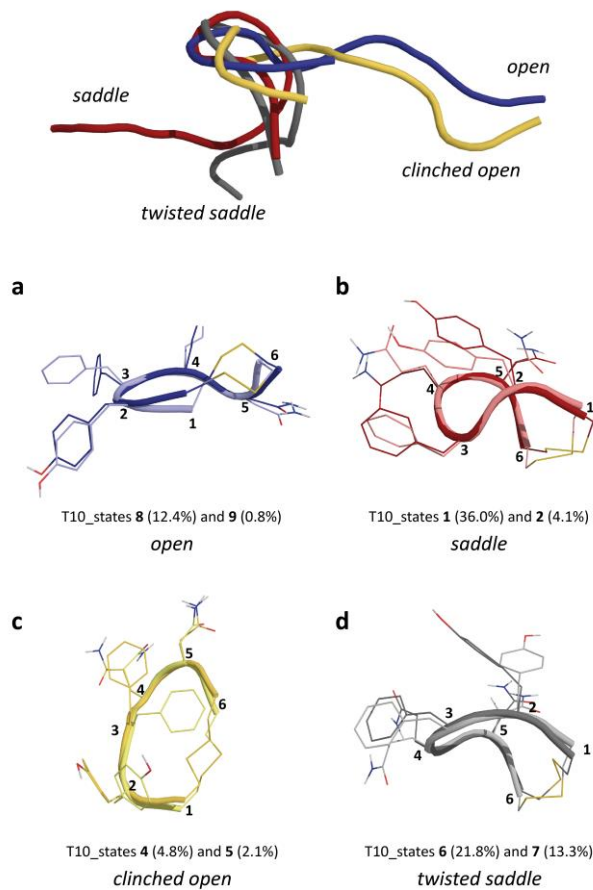


**Fig. 3**

Main ring conformations of 8-Arg-vasopressin

Main representative ring states in water resulting from a DASH state analysis of backbone dihedrals  $\Phi/\Psi$  2 to 6. Absolute population of each state during 11 $\mu$ s MD are given in parenthesis

**(a)** *open* ring states; **(b)** *saddle* ring states; **(c)** *clinched open* ring states; **(d)** *twisted saddle* ring states. Depiction: backbone = cartoon, sidechains = lines. Residues are only labelled for the major populated state each and the N-terminal tail is not shown in **(a)** to **(d)** for clarity. For illustration, a ring alignment of the backbone cartoons of the 4 main ring state (T10\_8,1,4,6) including the tail, is shown above **(a)** to **(d)**.

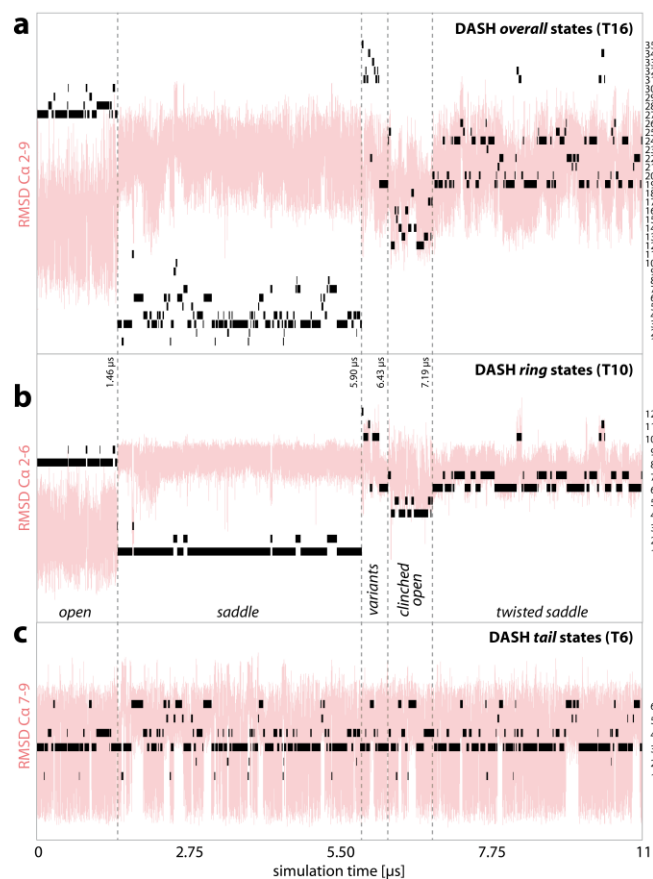


**Fig. 4**

DASH state trajectories for **(a) overall (T16)**, **(b) ring (T10)**, and **(c) tails (T6)** states

For a better understanding, the corresponding RMSD trajectories for *overall* (Ca 2 to 9), *ring* (Ca 2-6) and *tail* (Ca 7-9) alignments are shown in the background. States are numbered consecutively on the second y-axis, thus every horizontal line is the trajectory of a single DASH state and illustrates its individual distribution during the simulation. The transitions between time-windows of main ring conformations are marked with vertical dashed lines.

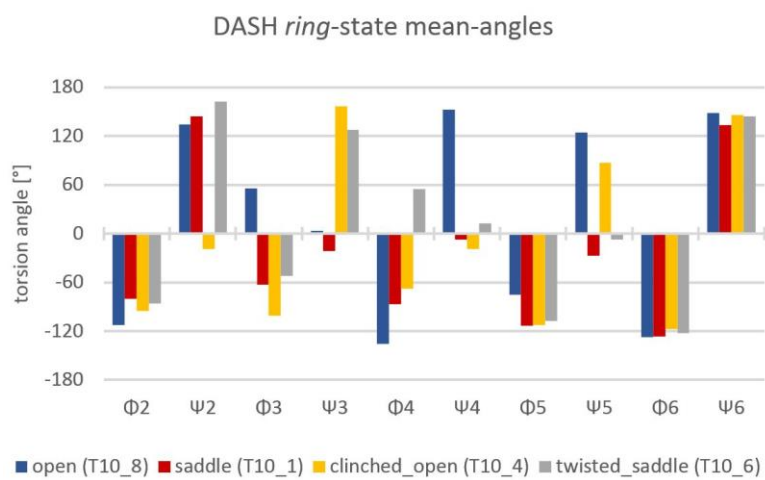


**Fig. 5**

DASH state mean angles ( $\Phi/\Psi$ ) of the main ring conformations of 8-Arg-vasopressin *open*, *saddle*, *clinched open*, and *twisted saddle* represented by the main ring states T10\_8, 1, 4, and 6



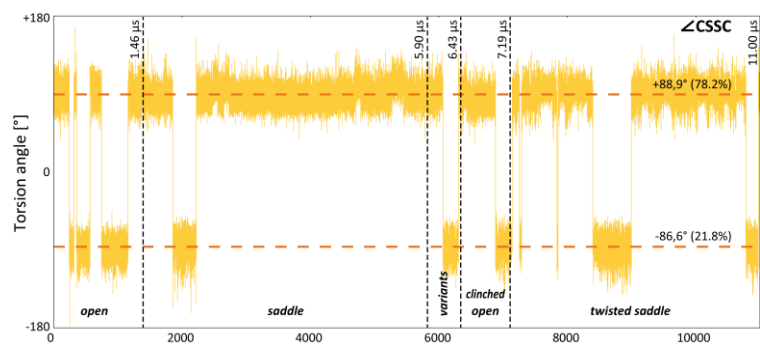


**Fig. 6**

Trajectory of the disulfide-bridge torsion Cys2 $\chi$ 3 ( $\angle$ CSSC)

Horizontal dashed lines = average disulfide bridge torsions, vertical dashed lines = transitions between time-windows of main ring conformations

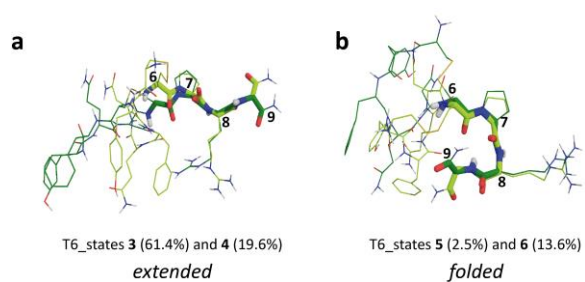


**Fig. 7**

Tail conformations of 8-Arg-vasopressin

Main representative tail states resulting from a DASH state analysis of backbone dihedrals  $\Phi/\Psi$  7 to 9. Absolute population are given in parenthesis. **(a)** *extended* tail conformations; **(b)** *folded* tail conformations with  $\beta$ -turn centered at residues 7 and 8. Depiction: tail = sticks, ring and side chains = lines. Residues are only labeled for each major populated state.

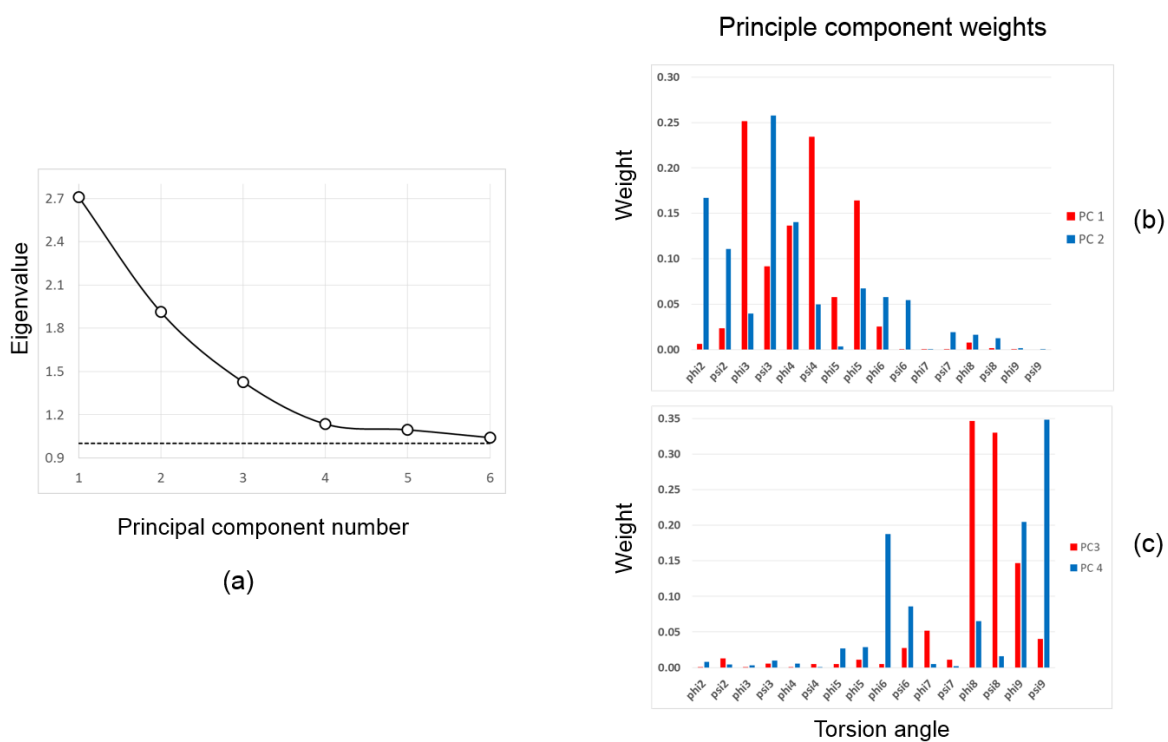


**Fig. 8**

Summaries of the principal component analysis of the torsion angles during the simulation

**(a)** Eigenvalue plot; **(b)** weights of the torsion angles for principal components 1 and 2; **(c)** weights of the torsion angles for principal components 3 and 4

## Tables

**Table 1** Average root mean square deviations (avRMSD) and average radii of gyration (avRadGyr) for significant trajectory time-windows and backbone C $\alpha$  alignments of 8-Arg-vasopressin

		trajectory time window [ $\mu$ s]				
		0-1.46	1.46-5.90	5.90-6.43	6.43-7.19	7.1-11.00
alignment		<i>open</i>	<i>saddle</i>	<i>variants</i>	<i>clinched open</i>	<i>twisted open</i>
avRMSD [ $\text{\AA}$ ]	<b><i>overall</i></b> <sup>a</sup>	1.825	2.930	2.683	2.274	2.756
	<b><i>ring</i></b> <sup>b</sup>	0.950	1.807	1.765	1.592	1.717
	<b><i>tail</i></b> <sup>c</sup>	0.991	1.157	1.102	1.164	1.068
avRadGyr [ $\text{\AA}$ ]	<b><i>ring</i></b>	4.077	3.278	3.569	3.870	3.500

<sup>a</sup>C $\alpha$  1-9 alignment; <sup>b</sup>C $\alpha$  1-6 alignment; <sup>c</sup>C $\alpha$  7-9 alignment. (Abbreviations see glossary)

**Table 2** Representative states of the main overall and ring conformations of 8-Arg-vasopressin

Listed are the population and conformational characteristics of the main overall states (T16) and ring states (T10) of AVP (minor and transient state variants: see Table S1). Absolute populations refer to 11  $\mu$ s MD (100%). Relative populations refer to the main time-windows of each conformational group (*open*, *saddle*, *clinched open* or *twisted saddle*). Characteristics of each ring conformation are given by  $\beta$ -turn types, turn centers, and transannular hydrogen bonds (Hbonds).

T16 State	State population (T16)		T10 State	State population (T10)		Conformational characteristics		
	abs [%]	rel [%]		abs [%]	rel [%]	$\beta$ -turn type <sup>a</sup>	Turn center	H bonds <sup>b</sup>
<i>open</i> (0 to 1.455 $\mu$ s = 1.455 $\mu$ s)								
<b>27</b>	8.62	64.74	<b>8</b>	12.40	93.75	no classical turns	2,3	(Tyr <sup>2</sup> O <sup>1</sup> Gln <sup>4</sup> NH)
<b>28</b>	3.25	24.60	<b>8</b>					
<b>29</b>	0.65	4.95	<b>8</b>					
<b>30</b>	0.75	5.70	<b>9</b>	0.83	6.25			
<b>total</b>	<b>13.28</b>	<b>100.00</b>		<b>13.23</b>	<b>100.00</b>			
<i>saddle</i> (1.455 to 5.900 $\mu$ s = 4.445 $\mu$ s)								
<b>1</b>	0.95	2.34	<b>1</b>	35.97	89.02	I/(I)	3,4/4,5	Tyr <sup>2</sup> OAsn <sup>5</sup> NH, Tyr <sup>2</sup> OCys <sup>6</sup> NH
<b>2</b>	0.74	1.82	<b>1</b>					
<b>3</b>	19.65	48.63	<b>1</b>					
<b>4</b>	7.88	19.51	<b>1</b>					
<b>5</b>	1.22	3.03	<b>1</b>					
<b>6</b>	5.60	13.87	<b>1</b>					
<b>7</b>	3.07	7.60	<b>2</b>	4.10	10.13			
<b>8</b>	0.35	0.87	<b>2</b>					
<b>9</b>	0.35	0.87	<b>2</b>					
<b>10</b>	0.25	0.62	<b>2</b>					
<b>total</b>	<b>40.06</b>	<b>99.15</b>		<b>40.07</b>	<b>99.16</b>			
<i>clinched open</i> (6.429 to 7.187 $\mu$ s = 0.758 $\mu$ s)								
<b>12</b>	1.87	27.18	<b>4</b>	4.80	69.66	(VIII) / I	4,5	(Phe <sup>3</sup> OCys <sup>6</sup> NH)
<b>13</b>	1.41	20.45	<b>4</b>					
<b>14</b>	1.45	20.98	<b>4</b>					
<b>15</b>	0.23	3.30	<b>5</b>	2.09	30.34			
<b>16</b>	0.89	12.93	<b>5</b>					
<b>17</b>	0.62	8.97	<b>5</b>					
<b>18</b>	0.43	6.20	<b>5</b>					
<b>total</b>	<b>6.89</b>	<b>100.00</b>		<b>6.89</b>	<b>100.00</b>			
<i>twisted saddle</i> (7.187 to 11.000 $\mu$ s = 3.813 $\mu$ s)								
19	14.04	36.32	<b>6</b>	21.8	57.62	II	3,4	Tyr <sup>2</sup> OAsn <sup>5</sup> NH
20	3.24	9.34	<b>6</b>					
21	0.85	2.44	<b>6</b>					
22	3.81	9.91	<b>6</b>					
23	0.26	0.76	<b>7</b>	13.33	37.11			
24	9.84	27.98	<b>7</b>					
25	2.07	5.01	<b>7</b>					
26	1	2.86	<b>7</b>					
<b>total</b>	<b>35.10</b>	<b>94.62</b>		<b>35.13</b>	<b>94.73</b>			
$\Sigma$ total	95.33			95.32				

T16 = overall states defined by  $\Phi/\Psi$  2 to 9; T10 = ring states defined by  $\Phi/\Psi$  2 to 6; <sup>a</sup>parentheses indicate distorted versions of ideal  $\beta$ -turn types; <sup>b</sup>Hydrogen bonds in parenthesis are only populated 20-40%; (Abbreviations see glossary)

**Table 3** DASH state mean angles ( $\Phi/\Psi$ ) of the main ring states (T10) of 8-Arg-vasopressinTorsions corresponding to  $\beta$ -turns are marked (dark grey = turn propensity > 80%, light grey = turn propensity 40-65%)

T10 state	Tyr <sup>2</sup> $\Phi$	Tyr <sup>2</sup> $\Psi$	Phe <sup>3</sup> $\Phi$	Phe <sup>3</sup> $\Psi$	Gln <sup>4</sup> $\Phi$	Gln <sup>4</sup> $\Psi$	Asn <sup>5</sup> $\Phi$	Asn <sup>5</sup> $\Psi$	Cys <sup>6</sup> $\Phi$	Cys <sup>6</sup> $\Psi$
<i>open</i>										
<b>8</b>	-112.54	134.53	55.31	3.41	-135.33	152.15	-75.09	124.68	-127.16	148.39
StdDev	37.81	18.46	9.08	31.34	23.92	18.2	18.32	32.08	31.88	23.33
<b>9</b>	-98.98	129.37	56.09	0.76	-135.73	153.49	-66.41	113.78	-55.29	126.93
StdDev	54.64	26.48	9.27	31.72	23.88	23.1	31.29	80.23	61.52	40.84
<i>saddle</i>										
<b>1</b>	-80.2	143.87	-62.88	-21.36	-86.73	-7.38	-113.37	-27.13	-126.42	133.12
StdDev	20.52	12.37	9.44	13.4	17.2	16.94	21.14	22.14	20.16	33.23
<b>2</b>	-84.29	147.09	-57.99	-27.01	-85.13	-7.63	-122.03	-6.72	-60.49	142.38
StdDev	23.05	13.93	10.95	15.59	17.53	16.62	20.55	41.47	32.18	24.51
<i>clinched open</i>										
<b>4</b>	-95.37	-19	-101.27	156.57	-67.65	-19.06	-112.46	86.89	-117.42	145.84
StdDev	28.15	22.75	29.46	14.56	16.85	23.84	28.66	61.3	36.21	21.54
<b>5</b>	-90.52	-18.35	-116.2	151.18	-68.06	-20.5	-88.17	14.01	-82.72	144.88
StdDev	28.3	18.64	30.65	13.16	22.02	26.74	20.39	33.03	29.6	16.17
<i>twisted saddle</i>										
<b>6</b>	-86.02	162.33	-52.48	127.66	55.04	12.34	-107.29	-7.44	-122.17	144.18
StdDev	29.44	13.88	16.16	14.69	9.01	21.14	29.86	48.29	28.23	23.53
<b>7</b>	-115.65	174.87	-52.78	129.79	57.39	8.38	-114.1	-16.45	-70.67	148.3
StdDev	24.26	19.63	19	13.91	8.24	20.56	25.07	29.84	19.33	13.72

Ideal  $\Phi/\Psi$  (i+1, i+2):  $\beta$ -turn type I (-60°, -30°, -90°, 0°), type II (-60°, +120°, +80°, 0°), type VIII (-60°, -30°, -120°, 120°)<sup>42</sup>. StdDev= standard deviation

**Table 4** Turn propensities [%] for the main ring conformations of 8-Arg-vasopressin

Turn center residue	Main ring conformation / Trajectory time-window			
	<i>open</i>	<i>saddle</i>	<i>clinched open</i>	<i>twisted saddle</i>
Cys <sup>1</sup>	0.00	0.00	0.00	0.00
Tyr <sup>2</sup>	20.20	0.00	0.00	0.18
Phe <sup>3</sup>	20.20	94.10	0.03	90.57
Gln <sup>4</sup>	0.08	93.93	46.28	93.80
Asn <sup>5</sup>	0.07	89.33	46.28	61.93
Cys <sup>6</sup>	0.00	2.53	0.00	0.01
Pro <sup>7</sup>	3.80	18.57	20.99	10.82
Arg <sup>8</sup>	3.80	17.32	20.99	10.82
Gly <sup>9</sup>	0.00	0.00	0.00	0.00

(Abbreviations see glossary)

**Table 5** Occupancies of intramolecular hydrogen bonds [%] and corresponding turn centers for the main ring conformations of 8-Arg-vasopressin

H-bond		Main ring conformation / Trajectory time-window				Turn center
O...	...HN	<i>open</i>	<i>saddle</i>	<i>cl.open</i>	<i>tw.saddle</i>	residues
Cys <sup>1</sup>	Gln <sup>4</sup>	12.03	0.00	0.00	2.24	2, 3
Tyr <sup>2</sup>	Asn <sup>5</sup>	0.00	95.70	0.00	82.60	3, 4
Tyr <sup>2</sup>	Cys <sup>6</sup>	0.00	83.19	0.00	37.28	3, 4, 5
Tyr <sup>2</sup>	Gln <sup>4</sup>	38.57	2.04	0.01	0.02	3
Phe <sup>3</sup>	Cys <sup>6</sup>	0.00	4.86	27.93	0.04	4, 5
Phe <sup>3</sup>	Asn <sup>5</sup>	0.13	2.41	10.21	23.83	4
Gln <sup>4</sup>	Cys <sup>6</sup>	8.78	0.06	18.67	1.60	5
Asn <sup>5</sup>	Tyr <sup>2</sup>	0.00	0.22	0.00	6.59	3, 4
Cys <sup>6</sup>	Gly <sup>9</sup>	2.20	10.82	12.11	5.67	7, 8



**Table 6** Population and distribution of tail conformations

The first column contains the DASH states (T6) that represent the tail conformations of 8-Arg-vasopressin during 11  $\mu$ s MD simulation. Absolute populations refer to the total simulation time of 11  $\mu$ s. Relative populations refer to the time-windows of the main ring conformation (*open*, *saddle*, *clinched open*, and *twisted saddle*).

T6 state	Tail state population (T6)				
	<i>open</i>	<i>saddle</i>	<i>clinched open</i>	<i>twisted saddle</i>	
	(0-11.0 $\mu$ s)	(0-1.46 $\mu$ s)	(1.46-5.90 $\mu$ s)	(6.43-7.19 $\mu$ s)	(7.19-11.00 $\mu$ s)
	abs [%]	rel [%]	rel [%]	rel [%]	rel [%]
<b><i>extended</i></b>					
<b>3</b>	61.44	69.22	56.02	37.99	68.34
<b>4</b>	19.59	24.39	20.32	30.35	15.10
total	81.03	93.61	76.34	68.34	83.44
<b><i>7,8 <math>\beta</math>-turn type II</i></b>					
<b>5</b>	2.52	0.00	3.87	0.00	2.75
<b>6</b>	13.61	4.91	15.31	26.12	12.51
total	16.13	4.91	19.18	26.12	15.26
<b><i>7,8 <math>\beta</math>-turn type I</i></b>					
<b>2</b>	0.83	0.00	1.82	0.00	0.28
<b><i>distorted turn</i></b>					
<b>1</b>	2.00	1.48	2.66	5.54	1.02
$\Sigma$ total	100.00	100.00	100.00	100.00	100.00

T6 = tail states defined by  $\Phi/\Psi$  7 to 9. (Abbreviations, see glossary)

**Table 7** Overall State = Ring State + Tail State

A matrix of overall states (T16) as combination of the ring and tail states (T10 and T6) that represent the main ring and tail conformations (*open*, *saddle*, *clinched open*, *twisted saddle*, *extended*, and *folded*). The states result from DASH analyses of torsions  $\Phi/\Psi$  2 to 9 (T16, overall states), 2 to 6 (T10, ring states) and 7 to 9 (T6, tail states). The assignment is based on the corresponding DASH state trajectories. PDBs of all states are provided in the Supplementary Material.

Overall states (T16) (T6 X T10)				Tail states (T6)			
				<i>extended</i>		<i>7,8 <math>\beta</math>-turn II</i>	
				61.4%	19.6%	13.6%	2.5%
				<b>3</b>	<b>4</b>	<b>6</b>	<b>5</b>
<b>Ring states (T10)</b>	<b><i>open</i></b>	12.4%	<b>8</b>	<b>27</b>	<b>28</b>	<b>29</b>	
		0.8%	<b>9</b>	<b>30</b>	<b>28</b>		
	<b><i>saddle</i></b>	36.0%	<b>1</b>	<b>3</b>	<b>4</b>	<b>6</b>	<b>5</b>
		4.1%	<b>2</b>	<b>7</b>	<b>8</b>	<b>10</b>	<b>9</b>
	<b><i>clinched open</i></b>	4.8%	<b>4</b>	<b>12</b>	<b>13</b>	<b>14</b>	
		2.1%	<b>5</b>	<b>16</b>	<b>17</b>	<b>18</b>	
	<b><i>twisted saddle</i></b>	21.8%	<b>6</b>	<b>19</b>	<b>20</b>	<b>22</b>	<b>21</b>
		13.3%	<b>7</b>	<b>24</b>	<b>25</b>	<b>26</b>	